Feshbach projection formalism for transmission through a time-periodic potential

Almas F. Sadreev*
L. V. Kirensky Institute of Physics, 660036 Krasnoyarsk, Russia
(Received 4 May 2012; revised manuscript received 14 August 2012; published 20 November 2012)

The Feshbach projection formalism is applied to consider quantum transmission through a tight-binding wire subject to a time-periodic potential. The wire is coupled with two leads via the coupling constant v_C. The periodicity of the potential implies an additional temporal dimension that reduces the problem to stationary transmission through an effectively two-dimensional lattice system. The non-Hermitian effective Hamiltonian is formulated. Thist allows us to trace the redistribution of resonance positions and resonance widths with the growth of v_C from the weak-coupling to the strong-coupling regime.

DOI: 10.1103/PhysRevE.86.056211 PACS number(s): 05.45.Mt, 72.10.−d, 73.63.−b, 72.30.+q

I. INTRODUCTION

The problem of electron, acoustic, or microwave transmission through quantum dots (QDs), billiards, cavities, etc., includes the QD and, at least, two half-infinite leads that open the QD. Therefore, an exact description of open QDs meets the mathematical problem of matching the wave functions of discrete and scattering states. The full Hilbert space is divided into two subspaces: subspace Q is formed by the discrete functions localized within the QD and vanishing outside of it, while the wave functions of subspace P are the extended eigenfunctions of the leads. Livshits [1], in 1957, and, independently, Feshbach, in 1958 [2], introduced the idea and the method of projection of the total Hilbert space onto the discrete states of subspace Q. That procedure first formulated the concept of the effective Hamiltonian defined in subspace P of discrete states. The effective Hamiltonian is not Hermitian, with discrete complex eigenvalues corresponding to resonance positions and widths [3–6]. In the context of the finite-difference method the effective Hamiltonian was developed in Refs. [7] and [8] (see Sec. III). The Feshbach projection method was defined for the stationary processes of transmission through the QD. In the present paper we develop this method for the time-periodic perturbation.

Our approach is based on the idea that the time-dependent Schrödinger equation can be considered as time independent in an extended Hilbert space, which was introduced by Sambe [9] for time-periodic Hamiltonians. Considering time as an extra coordinate in the extended Hilbert space [10,11], we transform the open, one-dimensional (1D), $d = 1$ QD subjected to time-periodic perturbation to a stationary open, $d + 1$ QD. If the original $d = 1$ QD is open via coupling with two 1D leads, then the effective $d + 1$ QD is coupled with $2(2M + 1)$ leads, where $2M + 1$ is the number of Floquet states. Thereby we derive a $d + 1$ effective non-Hermitian Hamiltonian similar to that formulated for the stationary system [7,8]. For computational purposes this approach is hardly advantageous over the standard methods discussed below. However, the complex eigenvalues of the effective Hamiltonian allow us to trace the evolution of resonances [3–6] with the variation of the parameters of the system.

To be specific, in the present paper we study the transmission through a periodically driven tight-binding chain of length N as being dependent on the coupling constant v_C between the 1D QD and the leads. In the weak-coupling regime $v_C \ll 1$ we obtain the double-barrier resonant tunneling structure. The continuum version of this case was considered by Stone *et al.* [12]. For $v_C = 1$ the system is equivalent to the periodically driven δ-function chain [13,14]. We consider the evolution of the resonance properties of a harmonic time-dependent chain not only in the regime of the DBRTS but also in the case of strong coupling [15–18]. Finally, we calculate the conductance of the QD versus the frequency and amplitude of the time-periodic perturbation.

II. TRANSMISSION THROUGH A PERIODICALLY DRIVEN IMPURITY

In what follows we measure the electron energy in terms of the characteristic energy $E_0 = \hbar^2/2mL^2$, where $L = a_0 N$ is the length of the $d = 1$ QD and a_0 is the numerical step. We start with the simplest model,

$$H = -\sum_{j=-\infty}^{\infty} v_j |j\rangle\langle j+1| + \text{H.c.} + 2\lambda \cos\omega t |0\rangle\langle 0|, \quad (1)$$

which allows analytical treatment of the problem. We set $v_j = 1$ except $v_{-1} = v_L$ and $v_0 = v_R$. Thus, we have a single dynamically driven impurity coupled with two continua, $C = L, R$, via the coupling constants v_C. Model (1) is the tight-binding analog of the time-periodic 1D Schrödinger equation of the form [12–14]

$$i\frac{\partial\psi(x,t)}{\partial t} = \left\{-\frac{\partial^2}{\partial x^2} + 2\lambda\delta(x)\cos\omega t\right\}\psi(x,t). \quad (2)$$

We present the solution of the Schrödinger equation as

$$\psi_j(t) = \sum_n \left[\sqrt{\frac{1}{2\pi \sin k_0}} e^{ikj - iEt} + \sqrt{\frac{1}{2\pi \sin k_n}} r_n e^{-ik_n j - i(E+n\omega)t}\right], \quad j \leqslant 0,$$

*almas@tnp.krasn.ru

$$\psi_0(t) = \sum_n \psi_n e^{-i(E+n\omega)t}, \quad j = 0,$$

$$\psi_j(t) = \sum_n \sqrt{\frac{1}{2\pi \sin k_n}} t_n e^{ik_n j - i(E+n\omega)t}, \quad j \geqslant 0, \qquad (3)$$

where r_n and t_n are the reflection and transmission amplitudes and

$$-2\cos k_n = E + n\omega. \qquad (4)$$

Substituting Eqs. (3) into the Schrödinger equation, after simple algebra we obtain the following equations for the reflection and transmission amplitudes:

$$t_n = v_R \psi_n, \quad r_n = v_L t_n - \delta_{n,0},$$
$$[\exp(ik_n)(2v_C^2 - 1) - \exp(-ik_n) - E_0]\psi_n$$
$$= 2i v_C \sin k \delta_{n,0} + \lambda(\psi_{n+1} + \psi_{n-1}).$$

We define the transmission probability as the ratio of the output current flow on the right of the $j = 0$ impurity site to the input flow. The current flow is defined as

$$J(j) = J_0 \overline{\mathrm{Im}[\psi^*(j)\psi(j+1)]}, \quad J_0 = \frac{e\hbar}{2m^* L}. \qquad (6)$$

Here $\overline{\cdots} = \frac{\omega}{2\pi}\int_0^{2\pi/\omega} \ldots dt$. Substituting Eqs. (3) into Eq. (6) we obtain the total conductance

$$G = \sum_n |t_n|^2. \qquad (7)$$

This expression reduces to the standard expression for the conductance in the continuum approximation [19]. It is valid for low temperatures, $kT \ll \hbar\omega$, and for an infinitesimally small dc voltage difference applied to the leads [7]. This inequality bounds the frequency of the time-dependent perturbation from below. Also, it is assumed that the leads are not subjected to the ac voltage. Comparing Eq. (7) to the Landauer-Bütticker formula for the multichannel conductance [7], one can see that the contributions $\sin \mathrm{Re}(k_n)|t_n|^2$ are the electron transmission probabilities for the left lead with the incident energy E to the right lead with absorption (emission) of n quanta of energy.

The finite range of the propagation band in the tight-binding model constitutes the difference between the continuum model, (2), and the discrete one, (1). Note that only sideband states located within $[-2,2]$ are open channels. For $|E + n\omega| > 2$ the states become evanescent, i.e., localized in the vicinity of the impurity. Therefore we obtain from Eq. (4) the following solutions:

$$e^{ik_n} = \begin{cases} -\frac{E+n\omega}{2} + i\sqrt{1-\left(\frac{E+n\omega}{2}\right)^2}, & \text{if} \quad |E+n\omega| < 2, \\ -\frac{E+n\omega}{2} + \sqrt{\left(\frac{E+n\omega}{2}\right)^2 - 1}, & \text{if} \quad E+n\omega > 2, \\ -\frac{E+n\omega}{2} - \sqrt{\left(\frac{E+n\omega}{2}\right)^2 - 1}, & \text{if} \quad E+n\omega < -2. \end{cases} \qquad (8)$$

In Fig. 2 we show the conductance of the model versus the incident energy in the propagation band $[-2,2]$ and the frequency ω for different values of the coupling constant v_C. One can see from Figs. 2(a)–2(c) that the resonance dips in the conductance at $n\omega = \pm(E-2)$, $n = 1,2,\ldots$, evolve into the resonance satellite peaks at $n\omega = E, n = 0, \pm 1, \pm 2, \ldots$, as the coupling constants decrease. In Fig. 2(d) we see that the resonance dips in the conductance reappear in the strong-coupling regime $v_C = 2$.

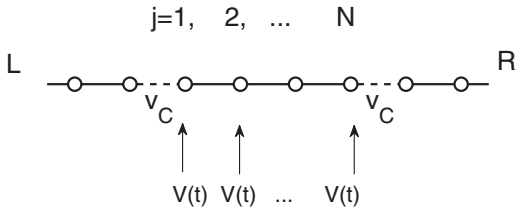

FIG. 1. Schematic of an N-site chain connected to semi-infinite wires via the hopping matrix element v_C. All other hopping matrix elements equal unity. Each site $j = 1,2,\ldots,N$ within the box is subject to the time-periodic potential $V(t) = 2\lambda\cos\omega t$.

Let us now consider the tight-binding chain of length N subject to the time-periodic potential as shown in Fig. 1. The total Hamiltonian of the chain with attached leads has the form

$$H = -\sum_{j=-\infty}^{0} |j\rangle\langle j+1| - \sum_{j=N+1}^{\infty} |j\rangle$$
$$\times \langle j+1| - v_C|0\rangle\langle 1| - v_C|N\rangle\langle N+1|$$
$$- \mathrm{H.c.} - \sum_{j=1}^{N} |j\rangle\langle j+1| + 2\lambda\cos\omega t \sum_{j=1}^{N} |j\rangle\langle j|, \qquad (9)$$

where the first two terms describe the leads (continua), the left and the right, the next two terms couple the chain to the leads, and the last term describes the chain. The case of $v_C = 1$ was considered in Ref. [10], where the conductance resonant dips were observed similarly to the case $N = 1$ shown in Fig. 2(a). Calculation of the reflection and transmission amplitudes is straightforward, similar to the previous case, $N = 1$, and is based on the fact that the chain is periodically driven as a whole. Then we can write the solution inside the chain in the form

$$\psi_j(t) = \sum_{n=-M_0}^{M_0} (a_n e^{ik_n j} + b_n e^{-ik_n j}) e^{-i(E+n\omega)t},$$
$$j = 1,2,\ldots,N, \qquad (10)$$

while the solution outside the chain has the same form as given in Eq. (3). Writing the Schrödinger equation for sites $j = 0,1$ and for $j = N, N+1$, one can obtain $4(2M_0+1)$ closed equations for r_n, t_n, a_n, and b_n, similar to those given in Ref. [8]. We skip this well-known procedure and go to the next section, where we calculate the transmission by use of the effective Hamiltonian.

III. GENERAL EQUATIONS

A. The Feschbach projection formalism for stationary transmission

Let H_B be the Hermitian Hamiltonian of a closed quantum system with the Dirichlet boundary conditions. The eigenvalue problem $H_B|b\rangle = E_b|b\rangle$ is assumed to be solved for the bound states $|b\rangle$ with the normalization condition $\langle b|b'\rangle = \delta_{bb'}$

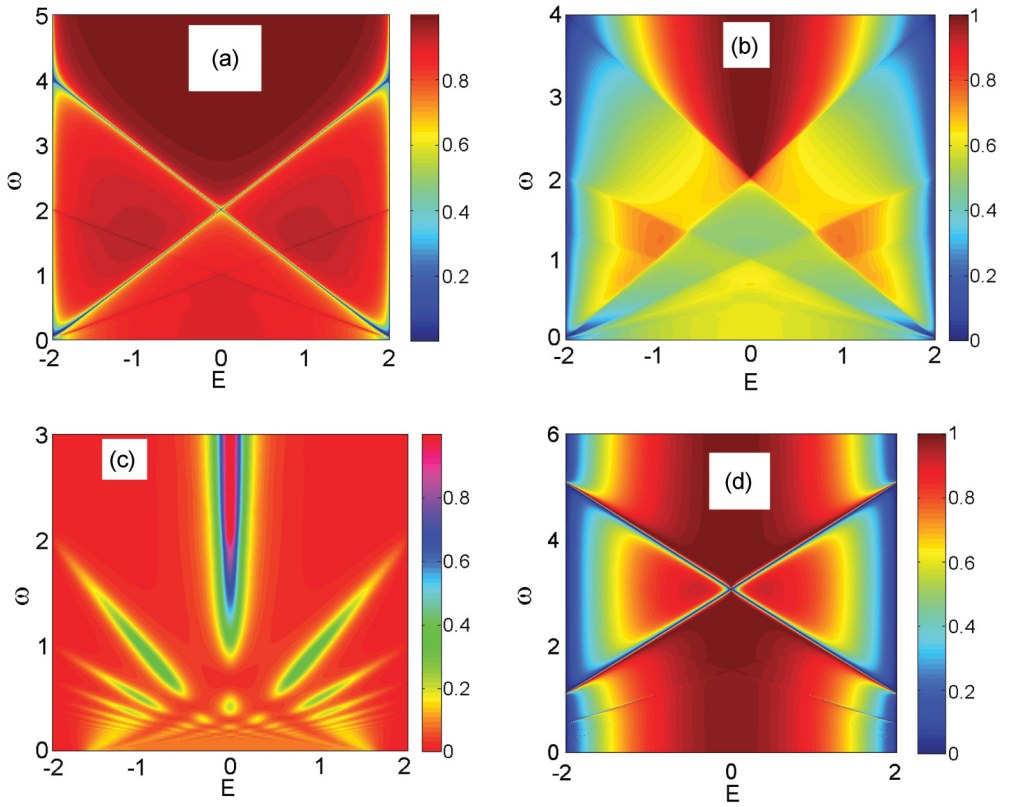

FIG. 2. (Color online) Conductance in the single-site model, (5), with $\lambda = 0.75$, $M_0 = 10$ versus the incident energy E and frequency ω for different values of the coupling constant v_C. (a) $v_C = 1$, (b) $v_C = 0.75$, (c) $v_C = 0.25$, and (d) $v_C = 2$.

and discrete eigenenergies E_b. When embedded into the continuum of scattering states, the discrete eigenstates of the closed system turn over into resonance states with a finite lifetime. These states are eigenstates of the effective non-Hermitian Hamiltonian $H_{\rm eff}$ of the open quantum system [3,4,6,15,20,21],

$$H_{\rm eff} = H_B + \sum_C V_{BC} \frac{1}{E^+ - H_C} V_{CB}. \tag{11}$$

Here V_{BC} and V_{CB} stand for the coupling matrices between the eigenstates of H_B and the environment that consist of different continua C. In the weak-coupling regime the complex eigenvalues of the effective Hamiltonian determine the positions and widths of the resonance states.

An evaluation of the transmission coefficient involves inversion of matrix $E - H_{\rm eff}$. For this one may use the site representation of Datta [7]. This approach is computationally efficient because the effective Hamiltonian is a sparse matrix. The second, physically more transparent way is to use the eigenstates of the closed system $H_B|b\rangle = E_b|b\rangle$ [8]. Here for the reader's convenience we explore a tutorial model of the 1D tight-binding chain with Hamiltonian (9) shown in Fig. 1. The eigenenergies and eigenfunctions of the chain of length N are the following:

$$E_n = -2\cos \pi n/(N+1), \quad n = 1,2,\ldots,N, \tag{12}$$

$$\psi_n(j) = \sqrt{\frac{2}{N+1}} \sin\left(\frac{\pi n j}{N+1}\right), \quad j = 1,2,\ldots,N. \tag{13}$$

The eigenfunctions of semi-infinite wires, left and right, are, respectively,

$$\psi_E(j) = \sqrt{\frac{1}{2\pi\rho(k)}} \sin k(1-j), \quad \psi_E(j) = \sqrt{\frac{1}{2\pi\rho(k)}} \sin k(N+1-j), \tag{14}$$

with the energy spectrum given by

$$E(k) = -2\cos k, \quad -\pi < k \leqslant \pi, \tag{15}$$

where $\rho(k) = dE/dk = 2\sin k$ is the density of states of the semi-infinite wire. The leads are attached to the chain at sites $j = 0, N+1$ via the hopping matrix element v_C, which is the coupling constant of the closed chain with two continua as shown in Fig. 1. In the site representation the Hamiltonian of chain H_B takes the standard form of two off-diagonals:

$$H_B = \begin{pmatrix} 0 & -1 & 0 & \cdots \\ -1 & 0 & -1 & \cdots \\ 0 & -1 & 0 & \cdots \\ \vdots & \vdots & \vdots & \cdots \end{pmatrix}. \tag{16}$$

The second contribution in Eq. (11) can be written as [7,8]

$$v_L^2 \langle 0| \frac{\sin^2 k}{E - H_C} |1\rangle = -v_L^2 e^{ik}, \tag{17}$$

where $v_L = \langle 0|V|1\rangle$. One can obtain the same expression for the coupling with the right lead. Therefore the second

contribution to the effective Hamiltonian is presented by only two diagonal terms given by the last term in Eq. (17). As a result, we obtain

$$H_{\rm eff}=\begin{pmatrix} -v_L^2e^{ik} & -1 & 0 & \cdots & 0 & 0\\ -1 & 0 & -1 & \cdots & 0 & 0\\ 0 & -1 & 0 & \cdots & 0 & 0\\ \vdots & \vdots & \vdots & \cdots & \vdots & \vdots\\ 0 & 0 & 0 & \cdots & 0 & -1\\ 0 & 0 & 0 & \cdots & -1 & -v_R^2e^{ik} \end{pmatrix}. \quad (18)$$

One can see that the effective Hamiltonian, (18), differs from the Hamiltonian of the closed chain, (16), by only two diagonal matrix elements.

B. The concept of the effective Hamiltonian for the time-periodic perturbation

We consider that the periodically oscillating potential

$$V_j(t)=2\lambda\cos\omega t,\quad j=1,2,\ldots,N, \quad (19)$$

is applied to the chain. Therefore we can present the wave function as

$$\psi_j(t)=\sum_m \psi_{m,j}e^{-i(E+m\omega)t}.$$

Then the Schrödinger equation for sites $j=0,1,\ldots,N,N+1$ gives us the following algebraic equations:

$$\begin{aligned}
&(E+m\omega)\psi_{m,0}+\psi_{m,-1}+v_C\psi_{m,1}=0,\\
&(E+m\omega)\psi_{m,1}+v_C\psi_{m,0}+\psi_{m,2}\\
&\quad-\lambda(\psi_{m+1,1}+\psi_{m-1,1})=0,\\
&(E+m\omega)\psi_{m,j}+(\psi_{m,j+1}+\psi_{m,j-1})\\
&\quad-\lambda(\psi_{j,m+1}+\psi_{j,m-1})=0,\\
&(E+m\omega)\psi_{m,N}+\psi_{m,N-1}+v_C\psi_{m,N+1}\\
&\quad-\lambda(\psi_{m+1,N}+\psi_{m-1,M})=0,\\
&(E+m\omega)\psi_{m,N+1}+\psi_{m,N+2}+v_C\psi_{m,N}=0.
\end{aligned} \quad (20)$$

Because of the time-periodic modulation the particle traveling through the chain can absorb and emit quanta of energy. Then the solution of the time-dependent Schrödinger equation in the leads can be written analytically [19,22–24],

$$\psi_j(t)=\begin{cases}\sum_m \frac{e^{-i(E+m\omega)t}}{\sqrt{2\pi\rho(k_m)}}\left[t_m^Le^{ik_mj}+r_m^Le^{-ik_mj}\right], & \text{left},\\ \sum_m \frac{e^{-i(E+m\omega)t}}{\sqrt{2\pi\rho(k_m)}}\left[t_m^Re^{ik_mj}+r_m^Re^{-ik_mj}\right], & \text{right},\end{cases} \quad (21)$$

where

$$E+m\omega=-2\cos k_m,\quad \rho(k_m)=\partial E/\partial k_m. \quad (22)$$

Substituting Eqs. (21) for sites $j=-1,0$ and $j=N+1$, $N+2$ into Eq. (20), one can link the incoming amplitudes t_m^L and t_m^R with the outgoing ones r_m^L and r_m^R via the Floquet scattering unitary matrix [19,23]. A similar approach was developed in Refs. [25] and [26] to account for temperature effects in the application to quantum pumping. In the present paper we present a different approach for the scattering matrix theory based on an equivalence of the time-periodic transmission through a d-dimensional lattice system to the stationary transmission through a $d+1$–dimensional system. Let us rewrite the Schrödinger equation for the stationary transmission through a 1D chain as follows:

$$\begin{aligned}
&E\psi_0+\psi_{-1}+v_C\psi_1=0,\quad E\psi_1+v_C\psi_0+\psi_2=0,\\
&E\psi_j+(\psi_{j+1}+\psi_{j-1})=0,\quad E\psi_N+\psi_{N-1}+v_C\psi_{N+1}=0,\\
&E\psi_{N+1}+\psi_{N+2}+v_C\psi_N=0.
\end{aligned} \quad (23)$$

Comparison of this equation with Eq. (20) shows that, first, Eq. (23) describes transmission through a two-dimensional (2D) lattice box with unit hopping matrix elements along the transport axis and with hopping matrix elements along the auxiliary temporal axis given by λ [27]. Moreover. the effective potential $V(m)=-\omega m$ is applied, which means a constant electric field ω directed along the temporal axis. That effective 2D box has numerical dimension $N\times(2M+1)$, where the second dimension $2M+1$ is the total number of sidebands. Generally, the temporal length of the billiard is infinite, however, in computations we take a finite M. A good accuracy of numerical computations is achieved for $M<\lambda/\omega$ [28]. Second, Eq. (20) shows that this effective 2D lattice box is coupled with $2M+1$ wires from both the left and the right as shown in Fig. 3. The eigenfunctions of the wires are

$$\begin{aligned}
\psi_m(j)&=\sqrt{\frac{1}{2\pi\rho_m(k)}}\sin k_m(1-j),\quad \rho_m(k)=2|\sin k_m|\\
&=2\sqrt{1-(E+m\omega)^2/4}.
\end{aligned} \quad (24)$$

Next, one can write the effective Hamiltonian for this open 2D box. For simplicity we present two cases: $N=1$ and $N=3$. For $N=1$ the effective 2D lattice box takes form

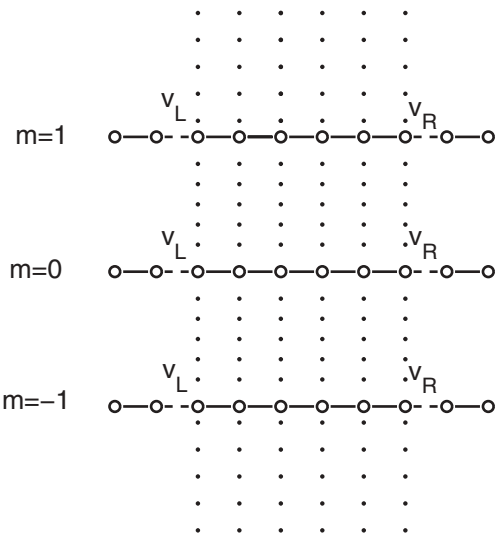

FIG. 3. Effective two-dimensional lattice box of $N(2M+1)$ sites connected to $2M+1$ semi-infinite wires. Each pair of left and right wires has the propagation band $E+m\omega=-2\cos k_m$. The unit hopping matrix elements along the chain are shown by solid lines, the hopping matrix elements λ along the temporal axis are shown by dotted lines, and the couplings between the semi-infinite wires and the box are shown by dashed lines.

of a vertical tight-binding chain of the length $2M+1$ with the hopping matrix element λ as shown in Fig. 4. In the site representation the Hamiltonian has the following form:

$$H_B = \begin{pmatrix} \ddots & \vdots & \vdots & \vdots & \vdots & \vdots & \\ \cdots & 2\omega & -\lambda & 0 & 0 & 0 & \cdots \\ \cdots & -\lambda & \omega & -\lambda & 0 & 0 & \cdots \\ \cdots & 0 & -\lambda & 0 & -\lambda & 0 & \cdots \\ \cdots & 0 & 0 & -\lambda & -\omega & 0 & \cdots \\ \cdots & 0 & 0 & 0 & -\lambda & -2\omega & \cdots \\ & \vdots & \vdots & \vdots & \vdots & \vdots & \ddots \end{pmatrix}. \quad (25)$$

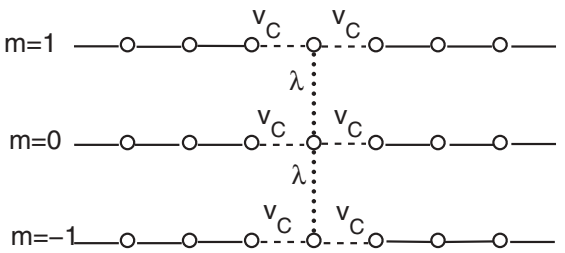

FIG. 4. Vertical chain of three temporal sites coupled via λ (dotted lines) and connected to three semi-infinite wires (dashed lines).

Respectively, we have for the effective Hamiltonian,

$$H_{\text{eff}} = \begin{pmatrix} \ddots & & & & & & \\ \cdots & 2\omega - 2v_C^2 e^{ik_2} & \lambda & 0 & 0 & 0\cdots & \\ \cdots & \lambda & \omega - 2v_C^2 e^{ik_1} & \lambda & 0 & 0 & \cdots \\ \cdots & 0 & \lambda & -2v_C^2 e^{ik_0} & \lambda & 0 & \cdots \\ \cdots & 0 & 0 & \lambda & -\omega - 2v_C^2 e^{ik_{-1}} & \lambda & \cdots \\ \cdots & 0 & 0 & 0 & \lambda & -2\omega - 2v_C^2 e^{ik_{-2}} & \cdots \\ & & & & & & \ddots \end{pmatrix}. \quad (26)$$

The factor 2 in terms $2v_C^2 e^{ik_m}$ is due to the fact that each site of the vertical chain is coupled with two wires as shown in Fig. 4.

Generalization to the case $N > 1$ is straightforward in accordance with Fig. 3. For example, if $N = 3$ and $M = 1$, we have

$$H_B = \begin{pmatrix} \omega & -1 & 0 & \lambda & 0 & 0 & 0 & 0 & 0 \\ -1 & \omega & -1 & 0 & \lambda & 0 & 0 & 0 & 0 \\ 0 & -u & \omega & 0 & 0 & \lambda & 0 & 0 & 0 \\ \lambda & 0 & 0 & 0 & -u & 0 & \lambda & 0 & 0 \\ 0 & \lambda & 0 & -u & 0 & -u & 0 & \lambda & 0 \\ 0 & 0 & \lambda & 0 & -u & 0 & 0 & 0 & \lambda \\ 0 & 0 & 0 & \lambda & 0 & 0 & -\omega & -u & 0 \\ 0 & 0 & 0 & 0 & \lambda & 0 & -u & -\omega & -u \\ 0 & 0 & 0 & 0 & 0 & \lambda & 0 & -u & -\omega \end{pmatrix} \quad (27)$$

and

$$H_{\text{eff}} = \begin{pmatrix} \omega - v_C^2 e^{ik_1} & -1 & 0 & \lambda & 0 & 0 & 0 & 0 & 0 \\ -1 & \omega & -1 & 0 & \lambda & 0 & 0 & 0 & 0 \\ 0 & -1 & \omega - v_C^2 e^{ik_1} & 0 & 0 & \lambda & 0 & 0 & 0 \\ \lambda & 0 & 0 & -v_C^2 e^{ik_0} & -1 & 0 & \lambda & 0 & 0 \\ 0 & \lambda & 0 & -1 & 0 & -1 & 0 & \lambda & 0 \\ 0 & 0 & \lambda & 0 & -1 & -v_C^2 e^{ik_0} & 0 & 0 & \lambda \\ 0 & 0 & 0 & \lambda & 0 & 0 & -\omega - v_C^2 e^{ik_{-1}} & -1 & 0 \\ 0 & 0 & 0 & 0 & \lambda & 0 & -1 & -\omega & -1 \\ 0 & 0 & 0 & 0 & 0 & \lambda & 0 & -1 & -\omega - v_C^2 e^{ik_{-1}} \end{pmatrix}. \quad (28)$$

Finally, we can write the scattering matrix similarly to the stationary case [4–6,8],

$$S_{C_m C'_{m'}} = \delta_{C_m C'_{m'}} - 2\pi i \langle E, C_m | V_{C_m B} \frac{1}{E - H_{\text{eff}}} V_{B C'_{m'}} | E, C'_{m'} \rangle = \begin{pmatrix} \widehat{R} & \widehat{T}' \\ \widehat{T} & \widehat{R}' \end{pmatrix}, \quad (29)$$

where matrix blocks $\widehat{T}$ and $\widehat{R}$ consist of elementary transmission and reflection coefficients t_{mn} and r_{mn}.

Let us introduce the biorthogonal basis [6,8],

$$H_{\text{eff}} |\mu) = z_\mu |\mu), (\mu|\mu') = \delta_{\mu,\mu'}, \quad |\mu) = |\mu>, \quad (\mu| =< \mu|^*. \quad (30)$$

Then the S matrix takes the following form:

$$S_{CC'} = \delta_{CC'}\delta_{mm'} - 2\pi i \sum_\mu \frac{\langle E, C_m | V_{CB} | \mu)(\mu | V_{BC} | E, C'_{m'} \rangle}{E - z_\mu}. \quad (31)$$

Equation (31) clearly shows that the transmission and reflection properties of the quantum system are given by complex eigenvalues z_μ and a coupling matrix with the continuum C, $\langle E,C|V_{CB}|\mu\rangle$ [8].

IV. NUMERICAL RESULTS

We start with the simplest case of a periodically driven site ($N = 1$). Surprisingly, even this case has turned out to be rather rich for variation of the coupling constant v_C.

The conductance given by Eq. (7) with $t_m = T_{0m}$ found from Eq. (29) is shown in Fig. 2. For the weak-coupling regime the resonances in the transmission are given by the eigenvalues of the vertical chain shown. In the chain with three vertical sites, $m = \pm 1,0$ (three side bands), shown in Fig. 4 the eigenvalues of Hamiltonian H_B can be written analytically:

$$E_b = 0, \pm\sqrt{\omega^2 + 2\lambda^2}. \tag{32}$$

These eigenenergies are plotted in Fig. 5(a) by solid lines. One can see that they well describe the frequency dependence of the resonances in the periodically driven site. In general the eigenvalues of Hamiltonian (25) can be written analytically only approximately near the band edge [29]. However, one can easily find the eigenvalues of Hamiltonian (25) numerically. The eigenvalues are plotted by solid lines in Figs. 6(b), 6(c), and 6(d) for $M = 2$, $M = 10$, and $M = 20$, respectively. The above cases are equivalent to stationary transmission through a vertical chain of length 3, 5, 21, and 41 sites, with 6, 10, 42, and 82, wires respectively. Figures 5(b) and 5(c) shows distinctively that an increase in the number $2M + 1$ of sidebands gives rise to a fine structure of the transmission probability located inside the rhombus-like domain $|\frac{E}{v_C} + \frac{\omega}{\lambda}| = 2$. Comparing the cases $M = 10$ and $M = 20$, one finds that the number of sidebands affects only the fine structure inside the rhombus-like domain, and does not change the transmission beyond. This agrees with the estimation of the number of sidebands necessary to accurately calculate the conductance $\omega \geqslant \lambda/M$ [28].

Let us see what happens with the growth of the coupling constant v_C. In the 1980s, a detailed investigation of this question was done in Ref. [15]. As v_C increases, the line widths grow as v_C^2, as seen from Eqs. (26) and (28), to give rise to overlapping of the resonances. That occurs when the resonance width reaches the mean distance between the eigenvalues of the closed system. In the limiting case of strong coupling $v_C \gg 1$, the results are governed by the algebraic structure of the anti-Hermitian part of the effective Hamiltonian [15]. Due to this structure, width bifurcation accompanied by a sharp redistribution of widths occurs at $\Gamma_r \geqslant 1$ [16,17]. As a result, K rapidly decaying states are formed, where K is the

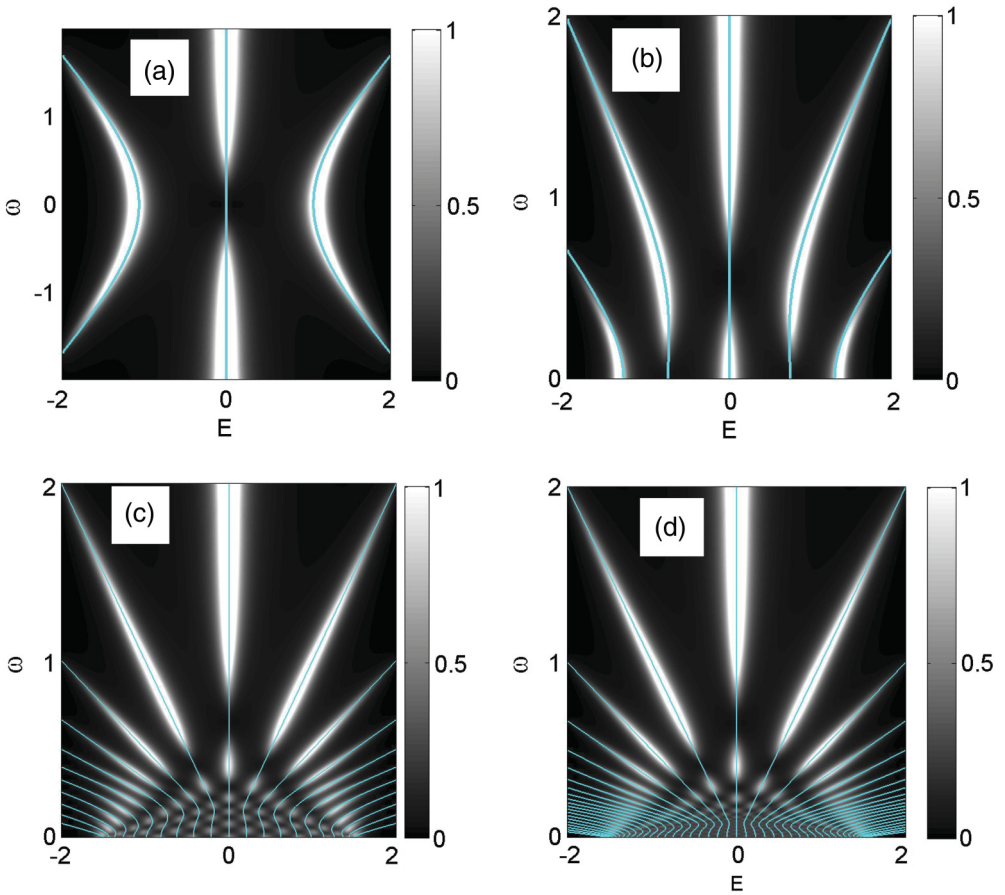

FIG. 5. (Color online) Conductance of a periodically driven single site with parameters $\lambda = 0.75$ and $v_C = 0.2$. The cases (a) of 3 sidebands, with $m = 0, \pm 1$, (b) of 5 sidebands, (c) of 21 sidebands, and (d) of 41 sidebands. Eigenenergies of Hamiltonian (25) are presented by solid lines.

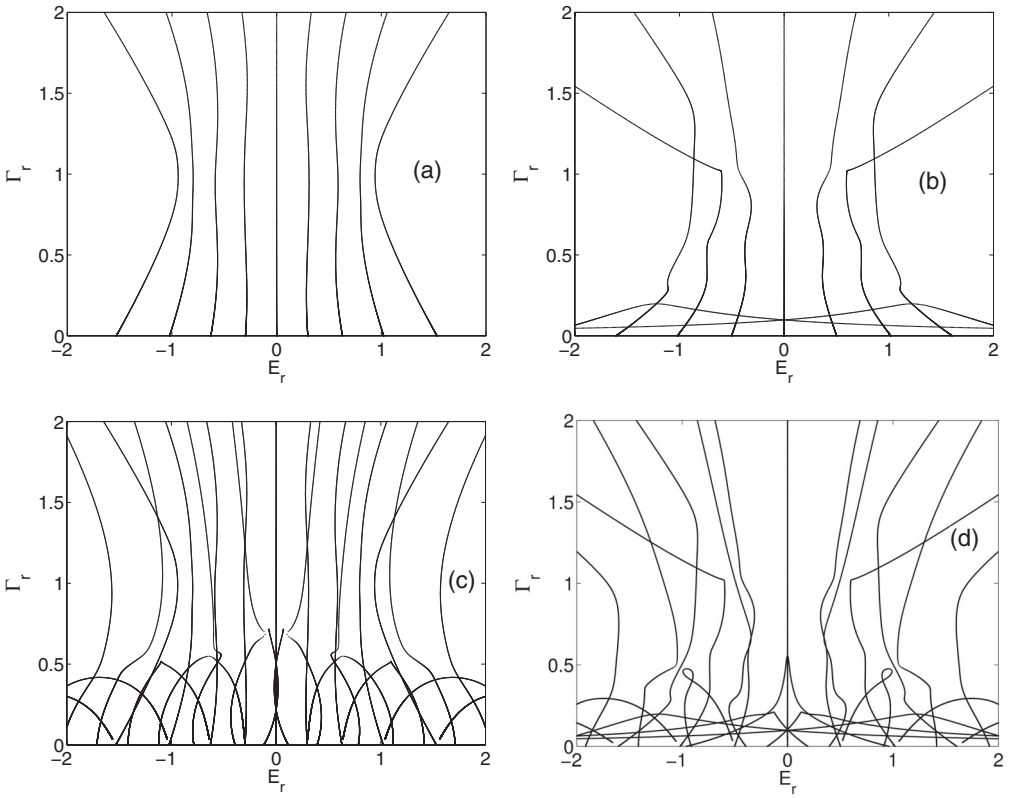

FIG. 6. Evolution of resonance positions $E_r = \mathrm{Re}(z)$ and resonance widths $\Gamma_r = -\mathrm{Im}(z)/2$ with growth of the coupling constant v_C from 0 to 5, where z are eigenvalues of the non-Hermitian effective Hamiltonian of a single periodically driven site $N = 1$ for $M = 4$, $\lambda = 0.5$, $E = 0$. (a) $\omega = 0.25$, $N = 1$, (b) $\omega = 0.5$, $N = 1$, (c) $\omega = 0.25$, $N = 3$, and (d) $\omega = 0.5$, $N = 3$.

number of open channels. The rest of the intermediate states are long-lived and have small excitation cross sections. An analysis of the width behavior as a function of the coupling constant is given in Ref. [18] in the case of a single open channel.

In our case of a periodically driven chain the number of open channels $K = 2(2M + 1)$, as one can see from Eqs. (26) and (28), while the dimension of the closed $d + 1$ box equals $N(2M + 1)$. Therefore, resonance trapping occurs with growth of the coupling constant when $N > 2$. That conclusion is illustrated in Fig. 6(a) for a chain with $N = 1$ and in Fig. 6(c) for a chain with $N = 3$ for the low frequency $\omega = 0.25$. However, for the higher frequency $\omega = 0.5$ the number of continua is restricted by the finite width of the propagation

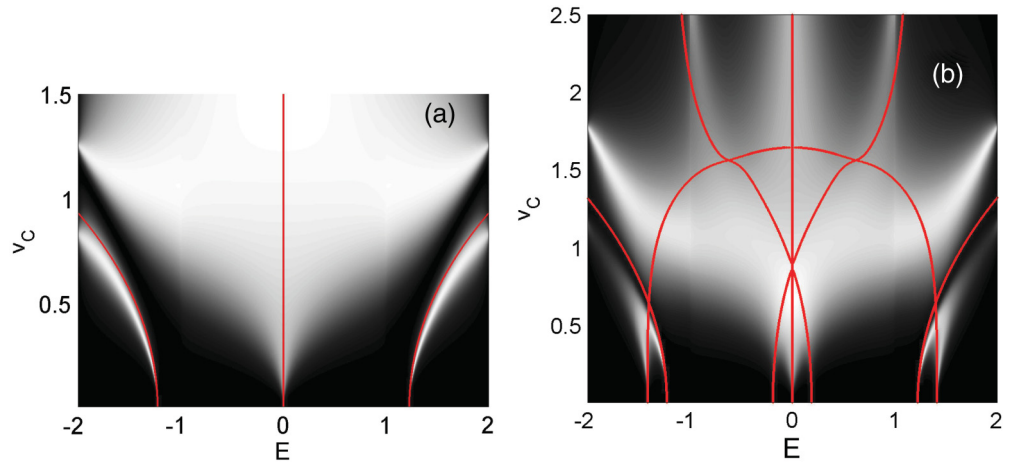

FIG. 7. (Color online) Conductance of a chain subject to the time-periodic perturbation $V(t) = \lambda \cos \omega t$ for $\lambda = 0.5$, $\omega = 1$ versus energy and the coupling constant v_C for (a) $N = 1$, $M_0 = 1$ and (b) $N = 3$, $M_0 = 1$. Resonance positions given as real parts of the complex eigenvalues of the effective Hamiltonian, (26) and (28), are shown by white lines. Eigenenergies of the Hamiltonian, (25) and (27), are shown by solid (red) lines.

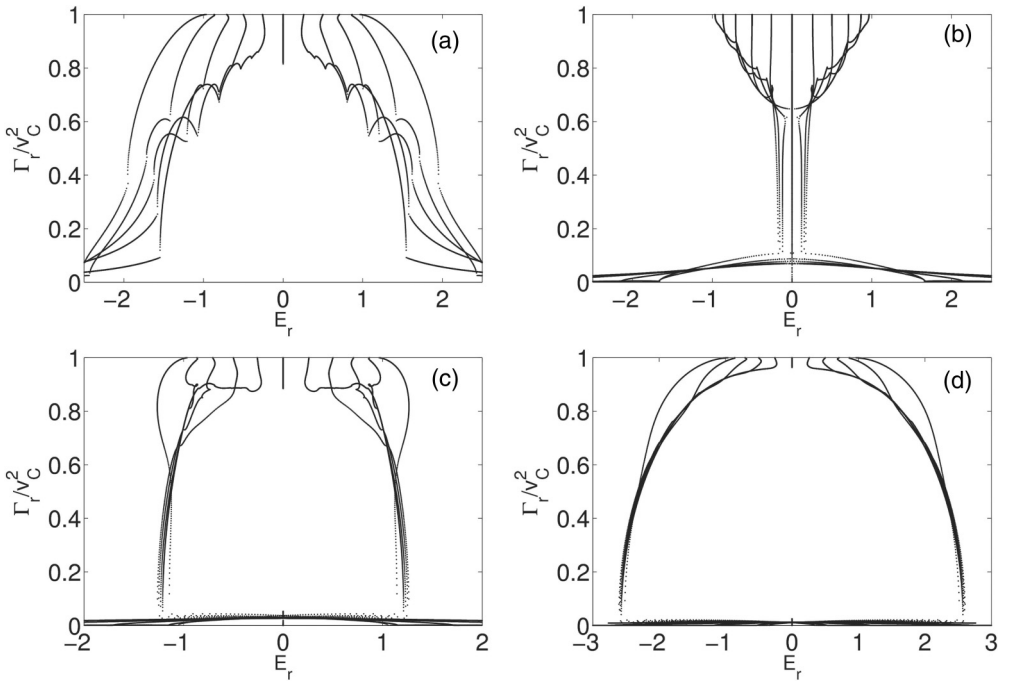

FIG. 8. Evolution of resonance positions $E_r = \mathrm{Re}(z)$ and resonance widths $\Gamma_r = -\mathrm{Im}(z)/2$ (normalized by v_C^2) as a function of frequency for different coupling constants v_C for $N = 1$, $M_0 = 5$, $\lambda = 0.5$, $E = 0$. (a) $v_C = 0.5$, (b) $v_C = 1$, (c) $v_C = 1.25$, and (d) $v_C = 1.5$.

band of the tight-binding leads $[-2,2]$. As soon as the sideband $E + n\omega$ goes beyond the principal band $[-2,2]$, it ceases to be a propagating channel. Respectively, the number of fast-decaying states is decreased compared to that at the lower frequency, as one can see from Figs. 6(b) and 6(d). For the low frequency ($\omega = 0.25$) all sidebands are inside the principal band, and therefore $K = 2(2M + 1) = 18$ resonances become very broad, while the rest, $2M + 1 = 9$ resonances, remain very narrow as illustrated in Fig. 7(c).

One can see from Fig. 7(a) that for a periodically driven single site, resonance positions given by real parts of the complex eigenvalues of the effective Hamiltonian (28) well describe the transmission peaks for $2v_C^2 < 1$ only, while for $v_C \gg 1$ there are no resonance peaks. However, when $N = 3$ the real parts of the complex eigenvalues well describe the transmission peaks not only for $2v_C^2 < 1$ but also for $v_C \gg 1$ as shown in Fig. 7(b). These numerical results illustrate the rules considered above. Here we are restricted by the minimal number of the sidebands in order to avoid a complicated behavior of eigenvalues of the effective Hamiltonian. Even in the case of three sidebands the $N = 3$ periodically driven chain displays a branching point at $E = 0$, $v_C = \sqrt{2}$ as shown in Fig. 7(b) (see details in Refs. [16], [17], and [30]). Figure 8 demonstrates the complicated behavior of resonance due to the finite band in the tight-binding wire at $v_C \approx 1$.

Figure 9 shows transmission vs frequency and amplitude of the time-periodic perturbation λ for two values of incident energy, $E = 0$ and $E = 1$. For a small coupling of the impurity site with the leads $E = 0$ the transmission peaks follow the eigenenergies of a closed vertical chain of length $2M + 1$

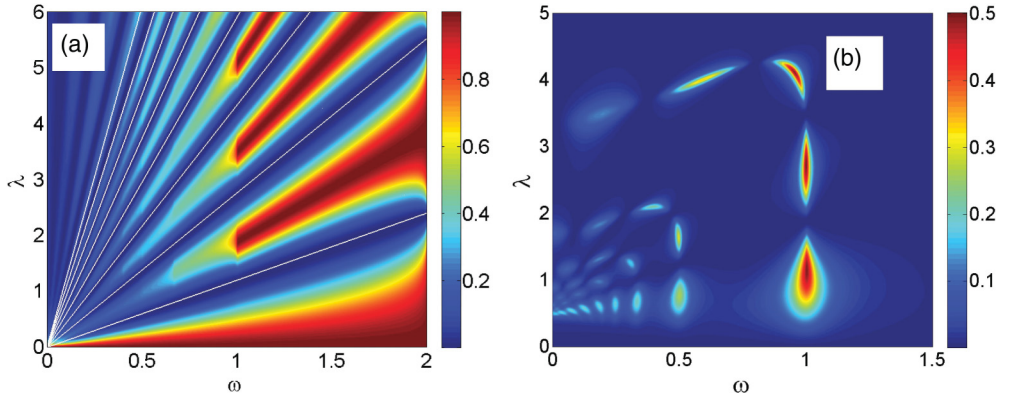

FIG. 9. (Color online) The transmission through a single impurity site versus the frequency and amplitude of oscillations for $v_C = 0.2$, $M_0 = 10$. (a) $E = 0$ and (b) $E = 1$. Zeros of the transmission shown by solid lines follow zeros of the Bessel function of the zeroth order, $J_0(2\lambda/\omega) \approx 0$ [31,32].

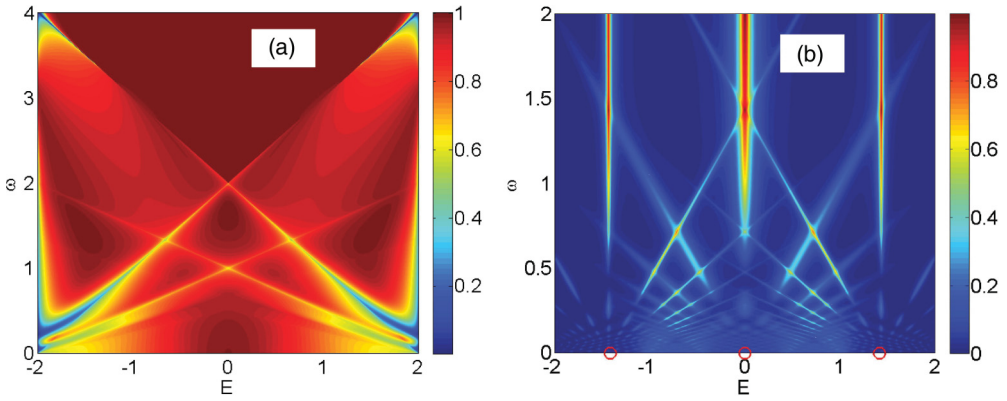

FIG. 10. (Color online) Conduction vs incident energy E and frequency ω for $N = 3$, $M_0 = 10$, $\lambda = 0.5$. (a) $v_C = 1$ and (b) $v_C = 0.25$. Open circles show eigenenergies of a closed chain with $N = 3$.

with the hopping matrix λ which are given by Eq. (32) for $M = 1$.

For $E = 0$ the transmission zeros in Fig. 9(a) are in full agreement with the results of Wagner [31,32]. However, for $E = 1$ the transmission zeros do not behave simply as Fig. 9(b) shows. Conduction vs energy and frequency in the case $N = 3$ is shown in Fig. 10. Similarly to the case $N = 1$ shown in Fig. 2(a), there are only slightly prominent resonance dips. However, in the weak-coupling regime one can see distinctive resonance sheaf structures, each originated from the eigenenergies of the chain $N = 3$ shown in Fig. 10(b) by open circles.

V. SUMMARY AND DISCUSSION

The Büttiker-Landauer conductance of a QD can be defined by the Green's function, which is an inversion of $E - H_{\text{eff}}$ where the effective non-Hermitian Hamiltonian is the result of projection of the full Hermitian Hamiltonian onto the eigenstates of a closed QD. The ac gate potential in a QD can transfer an incident electron of energy E to sidebands at $E + n\omega$, $n = -M, -M+1, \ldots, M-1, M$. Although the number of continua is increased by $2M + 1$ times, the Feshbach projection technique can be applied to give rise to an H_{eff} of dimension $(2M + 1)N$, with N the number of states of the QD. In this paper we derived the H_{eff} for some simple cases of tight-binding 1D QDs (chains) with a restricted number of sites subject to the harmonically driven potential. One can see that the matrix of H_{eff} given by Eqs. (26) and (28) has a simple banded structure.

We introduced the parameter v_C, which is the coupling constant between the closed QD and the leads. Although our approach in the case $v_C = 1$ reproduces results established before, it reveals an advantage of the effective Hamiltonian in the regimes of a weak and a strong coupling constant. It provides an opportunity to interpret numerical results (Figs. 7 and 10) in terms of the complex eigenvalues z of the effective Hamiltonian. $\text{Re}(z)$ is the position of a resonance peak, with the resonance width given by $-\text{Im}(z)/2$. That statement is obvious for $v_C \ll 1$ when the radiation shifts are small. Interestingly, the resonance peaks also follow $\text{Re}(z)$ in the strong-coupling regime $v_C \gg 1$ as shown in Fig. 7(b).

ACKNOWLEDGMENTS

I am grateful to Ingrid Rotter and Dmitrii Maksimov for discussions and critical reading of the manuscript.

[1] M. S. Livshits, Sov. Phys. JETP **4**, 91 (1957).
[2] H. Feshbach, Ann. Phys. (NY) **5**, 357 (1958); **19**, 287 (1962).
[3] I. Rotter, Rep. Prog. Phys. **54**, 635 (1991).
[4] F. M. Dittes, Phys. Rep. **339**, 215 (2000).
[5] D. V. Savin, V. V. Sokolov, and H.-J. Sommers, Phys. Rev. E **67**, 026215 (2003).
[6] I. Rotter, J. Phys. A: Math. Gen. **42**, 153001 (2009).
[7] S. Datta, *Electronic Transport in Mesoscopic Systems* (Cambridge University Press, Cambridge, 1995).
[8] A. F. Sadreev and I. Rotter, J. Phys. A: Math. Gen. **36**, 11413 (2003).
[9] H. Sambe, Phys. Rev. A **7**, 2203 (1973).
[10] S. Kohler, J. Lehmann, and P. Hänggi, Phys. Rep. **406**, 379 (2005).
[11] U. Peskin and N. Moiseyev, J. Chem. Phys. **99**, 4590 (1993).
[12] A. D. Stone, M. Ya. Azbel, and P. A. Lee, Phys. Rev. B **31**, 1707 (1985).
[13] M. Ya. Azbel, Phys. Rev. B **43**, 6847 (1991).
[14] D. F. Martinez and L. E. Reichl, Phys. Rev. B **64**, 245315 (2001).
[15] V. V. Sokolov and V. G. Zelevinsky, Nucl. Phys. A **504**, 562 (1989); Ann. Phys. **216**, 323 (1992).
[16] I. Rotter and A. F. Sadreev, Phys. Rev. E **69**, 066201 (2004).
[17] I. Rotter and A. F. Sadreev, Phys. Rev. E **71**, 036227 (2005).
[18] C. M. Jung, M. Müller, and I. Rotter, Phys. Rev. E **60**, 114 (1999).
[19] W. Li and L. E. Reichl, Phys. Rev. B **60**, 15732 (1999).
[20] C. Mahaux and H. A. Weidenmüller, *Shell Model Approach in Nuclear Reactions* (North-Holland, Amsterdam, 1969).
[21] V. V. Fyodorov and H.-J. Sommers, J. Math. Phys. **38**, 1918 (1997).

[22] P. K. Tien and J. P. Gordon, Phys. Rev. **129**, 647 (1963).
[23] C. P. del Valle, R. Lefebvre, and O. Atabek, Phys. Rev. A **59**, 3701 (1999).
[24] R. Lefebvre and N. Moiseyev, Phys. Rev. A **69**, 062105 (2004).
[25] M. Moskalets and M. Buttiker, Phys. Rev. B **66**, 205320 (2002).
[26] M. Moskalets and M. Buttiker, Phys. Rev. B **69**, 205316 (2004).
[27] A. F. Sadreev and K. Davlet-Kildeev, Phys. Rev. B **75**, 235309 (2007).
[28] E. N. Bulgakov and A. F. Sadreev, J. Phys.: Condens. Matter **8**, 8869 (1996).
[29] H. Fukuyama, R. A. Bari, and H. C. Fogedby, Phys. Rev. B **8**, 5579 (1973).
[30] E. N. Bulgakov, I. Rotter, and A. F. Sadreev, Phys. Rev. E **74**, 056204 (2006).
[31] M. Wagner and W. Zwerger, Phys. Rev. B **55**, R10217 (1997).
[32] M. Wagner, Phys. Rev. B **57**, 11899 (1998).